**Доклади на Българската академия на науките**
**Comptes rendus de l'Académie bulgare des Sciences**
*Tome 78, No 10, 2025*

*MEDICINE*
*Immunology*

# ASC DYNAMICS ASSOCIATED WITH ORF3a PROTEIN EXPRESSION IN MICROVASCULAR LUNG ENDOTHELIAL CELLS

**Yuliia Mariienko[1], Diana Pendicheva[2], Soren Hayrabedyan[1]✉, Krassimira Todorova[1,2]**

*Received on September 4, 2025*
*Accepted on September 30, 2025*

**Abstract**

The NLRP3 inflammasome is a key sensor of cellular stress and pathogen-associated signals in the innate immune system. Using confocal fluorescence microscopy in microvascular lung endothelial cells, we examined ASC speck formation following expression of the SARS-CoV-2 ORF3a protein. ORF3a engaged caspase-1 through dual architectural modes: alongside the canonical pyroptosome-like pathway, a novel distributed, multifocal inflammasome pathway emerged. Multiple ASC specks were observed at later time points, yet caspase-1 activation could occur in their absence, indicating that visible speck assembly is not strictly required for inflammasome signalling. These observations provide insight into the spatiotemporal dynamics of ASC during viral protein expression. The findings contribute to a better understanding of NLRP3 inflammasome regulation under conditions of viral replication.

**Key words:** ASC, ORF3a, inflammasome

**Introduction.** Inflammasomes are intracellular multiprotein complexes that assemble in response to microbial, host-derived, or environmental stimuli, leading to the activation of caspase-1. Activated caspase-1 proteolytically processes

This work was supported by the European Union-NextGenerationEU, through the National Recovery and Resilience Plan of the Republic of Bulgaria, Grant No BG-RRP-2.004-0003 and utilized equipment funded by National Roadmap for Research Infrastructure of the Ministry of Education and Science of Republic of Bulgaria, Grant No DO1-361/29.07.2022 and Grant No DO1-352/13.12.2023.

https://doi.org/10.7546/CRABS.2025.10.09

the proforms of IL-1β and IL-18, cytokines that play pivotal roles in innate immunity and inflammatory responses. In addition, caspase-1 cleaves gasdermin D, whose pore-forming activity facilitates the release of IL-1β and triggers pyroptotic cell death. The NLRP3 sensor protein oligomerizes upon activation and recruits the adaptor protein ASC (apoptosis-associated speck-like protein containing a CARD), which subsequently engages and activates caspase-1, establishing a functional inflammasome signalling platform [1, 2].

A canonical trigger of inflammasome activation follows a two-step mechanism: priming with lipopolysaccharide (LPS) via TLR4 signalling, which induces transcription of NLRP3 and pro-IL-1β, followed by a second signal such as extracellular ATP or nigericin that activates the NLRP3 inflammasome [3, 4]. Recent studies have demonstrated that ASC specks, while typically assembling as a single perinuclear punctum ($\sim$ 0.8–1 µm in diameter) in activated cells, can vary in number per cell, and caspase-1 activation frequently occurs in multiple smaller cytoplasmic complexes, not solely within the speck itself. In LPS/ATP-stimulated cells, one large ASC speck is commonly observed, whereas more potent stimuli can induce the formation of multiple ASC aggregates. Notably, active caspase-1 is often detected in dispersed cytoplasmic clusters, indicating that the large ASC speck functions as a signalling hub but is not the exclusive site of inflammasome activation [1]. Recent evidence further implicates viral proteins, such as SARS-CoV-2 ORF3a, in mimicking this canonical pathway as it functions as a viroporin, thereby promoting NLRP3 inflammasome activation, stimulating ASC speck formation, and triggering caspase-1 activation [5, 6].

**Materials and methods.** ***Cell culture.*** Microvascular endothelial cells isolated from human lung (Hulec-5a from American Type Culture Collection (ATCC)) were cultured in Endothelial cell line medium (ECM, Innoprot, Spain) designed for optimal growth of normal primary microvascular endothelial cells in vitro and contains fetal bovine serum 5%, 1% endothelial cell growth supplement, 1% penicillin/streptomycin solution. The medium is bicarbonate buffered and has a pH of 7.4.

***Plasmid DNA transfection.*** Hulec-5a was transfected when the 70% confluency was reached with 0.1 µg/µl of the SARS-CoV-2 ORF3a-mRFP (NCBI Reference Sequence: YP_009724391.1), isolated from SARS-CoV-2 Wuhan-Hu-1 and inserted into the SgfI-MluI restriction sites of the pCMV6-AC-mRFP expression vector (OriGene, Rockville, MD, USA) or/and 0.2 µg/µl of the ASC (NCBI Reference Sequence: NP_037390.1), inserted into the pRP-LmCerulean expression vector (Addgene, Watertown, MA, USA). The transfection complex was prepared at a 1:3 DNA:transfectant 8.0 (OriGene, Rockville, MD, USA) ratio and maintained according to the manufacturer's instructions. The transfection continued for 24 h at 37 °C and 5% $CO_2$.

***Caspase-1 activity detection.*** The FAM-FLICA® Assay Kit (Immuno-Chemistry Technologies, USA) was used to detect caspase-1 activity. The FLICA

reagent FAM-YVAD-FMK was added in ratio 1:30 to the medium and incubated for 45 min at 37 °C and 5% $CO_2$. The reagent efficiently diffuses across the cell membrane and binds covalently irreversibly to the Tyr-Val-Ala-Asp (YVAD) sequences of active caspases-1, generating a fluorescent signal that is excited at 492 nm and emitted at 520 nm. Unbound FLICA diffused out of the cell during the washing steps with 1× apoptosis wash buffer from the kit after incubation. Positive control for caspase-1 activity was created, using 1 µg/ml lipopolysaccharide (LPS) for 3 h followed by nigericin at 10 µM for 1 h at 37 °C and 5% $CO_2$. As negative control non-treated cells grown in a normal cell culture environment were used.

***YoPro-1 cell-viability assay.*** Immediately prior to imaging, culture medium was replaced with pre-warmed ECM containing Yo-Pro at 0.5 µM and cells were incubated 10 min at 37 °C, protected from light, and imaged without fixation.

***Confocal imaging and post-processing.*** Imaging was initiated immediately after the addition of the transfection mix by confocal spinning disk microscopy BC43 (Andor, Oxford instruments, UK). The experiment was conducted under maintained conditions (37 °C, 5% $CO_2$). Image acquisition for all conditions was performed with 40× objective magnification. Excitation/emission: Hoechst (Ex 405 nm/Em 430–480 nm), YoPro-1 (Ex 488–491 nm/Em 500–550 nm), mRFP-ORF3a (Ex 561 nm/Em 580–650 nm), Cerulean-ASC (Ex 445–458 nm/Em 465–510 nm). Image post-processing was performed using CellProfiler (version 5.0, Broad Institute). The analysis pipeline included the *Images*, *Metadata*, *NamesAndTypes*, *ColorToGray*. The mRFP (red) channel was used to identify ORF3a expression, the *FAM-FLICA channel* (green) represented active caspase-1 signal, *brightfield* (BF) channel for whole-cell segmentation, The *LmCerulean* (blue) channel was used to identify ASC formation. Fluorescent signal segmentation was done using *RunCellpose* modules from the appropriate channels. *IdentifyPrimaryObjects* was used to segment ORF3a expression based on the mRFP signal. *RelateObjects* modules were used to associate each cell with mRFP signal (transfected cell) or YoPro-1 with ASC and/or caspase-1 signal. Final measurements were exported using *ExportToSpreadsheet*.

***Statistics.*** A binomial generalized linear model (GLM) with logit link was applied to assess the effects of treatment (LPS vs. ORF3a) and time on the probability of ASC speck-positive cells. For transfection/activation analysis, we quantified the number of cells per field positive for ORF3a-mRFP, caspase-1 (FAM-FLICA), ASC (specks), and their combinations. Fractions were computed relative to the total number of cells per field. Binomial GLMs (*logit* link) were fitted with outcomes defined as marker-positive versus marker-negative cells, and for multi-marker analysis, triple- versus double-positive fractions within the ORF3a+ population. Models were implemented in Python (*statsmodels*).

**Results.** In both experimental conditions, ASC aggregation correlated with morphological changes in endothelial cells, including cell swelling and membrane

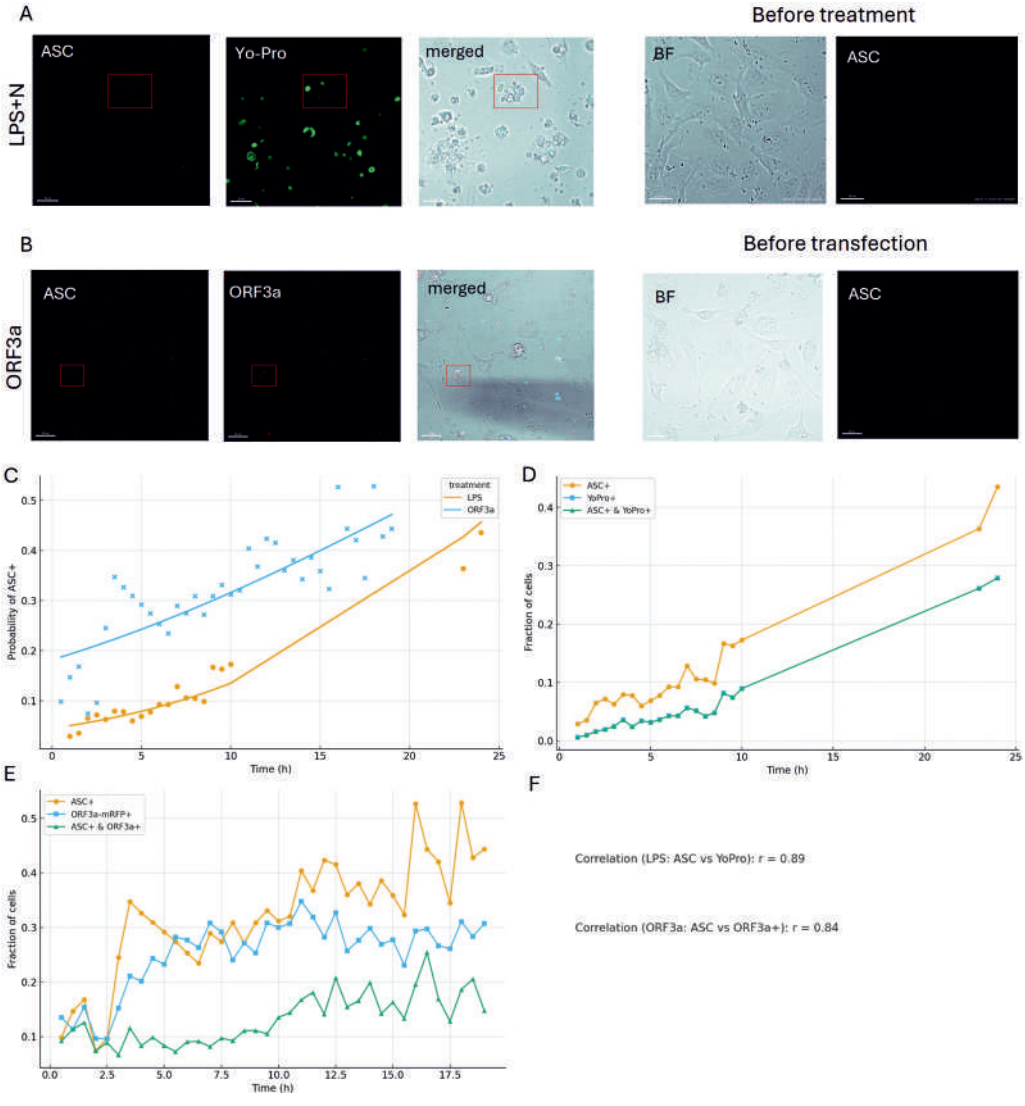


Fig. 1. (A, B) Representative pictures of experimental setup. Scale bar, 30 $\mu$m. (C) Observed ASC+ fractions (points) and fitted probabilities (lines) from a binomial GLM with logit link that included treatment (LPS vs. ORF3a), standardized time, and their interaction; the model was fit to field-level counts at each time point; no confidence bands are shown. The fit captures the higher baseline ASC+ probability under ORF3a and the steeper time-dependent increase under LPS (full coefficients reported in Table 1A). (D) ASC and YoPro-1 fractions over time. Time-lapse high-content imaging of Hulec-5a cells stimulated with LPS showing, at each time point, the fractions (% of all cells in the field) of ASC-positive cells ($\geq$ 1 ASC speck/cell), YoPro-1-positive cells (membrane-compromised/dead), and double-positive cells (ASC+/YoPro-1+). Fractions were computed as counts divided by the total number of segmented cells per field (range 147–1002 cells/field across time points). The ASC+ fraction here includes both single- and multi-speck cells. (E) ASC and ORF3a fractions over time. Time-lapse imaging of HULEC5a cells transfected with ORF3a-mRFP showing fractions (% of all cells) of ASC-positive cells ($\geq$ 1 speck), ORF3a-mRFP-positive cells (transgene-expressing), and double-positive cells (ASC+/ORF3a+). Fractions use the same denominator (total cells per field; range 124–203 cells/field); the ASC+ fraction likewise aggregates single- and multi-speck cells (the internal composition is detailed in the 100% stacked panels)

rupture (Fig. 1A). The graphs illustrate significantly higher baseline probability of ASC speck formation under ORF3a transfection compared to LPS stimulation, with time exerting a stronger effect in the LPS condition and a plateau-like dynamic under ORF3a (Fig. 1C, D, E). The GLM demonstrated that ORF3a-mRFP+ cells were significantly more frequent than YoPro+ cells under LPS (OR $\approx$ 3.1, 95% CI 2.8–3.4, $p < 0.001$). Time had a strong positive effect (OR $\approx$ 2.0, 95% CI 1.9–2.2, $p < 0.001$), while the time $\times$ ORF3a interaction was negative (OR $\approx$ 0.8, 95% CI 0.7–0.8, $p < 0.001$), consistent with rapid early accumulation of ORF3a+ cells followed by stabilization (Table 1A).

Table 1

Statistical model coefficients and significance values. (A) Binomial GLM (logit) comparing YoPro-1+ cells under LPS stimulation versus ORF3a-mRFP+ cells under ORF3a transfection, modelling the probability of functional marker positivity among all cells. (B) ASC speck composition. Binomial GLM (logit) modelling the probability of $\geq$2 specks versus 1 speck within ASC-positive cells, comparing LPS stimulation and ORF3a transfection. (C) ORF3a transfection efficiency and caspase-1 activation markers. Binomial GLM (logit) modelling the probability of marker-positive cells versus all cells across imaging fields

| Predictor | Coeff. | Std Error | $Z$ value | $p$ value | CI lower | CI upper | OR | OR CI lower | OR CI upper |
|---|---|---|---|---|---|---|---|---|---|
| A | | | | | | | | | |
| Intercept | −1.995 | 0.037 | −53.34 | 0 | −2.068 | −1.922 | 0.14 | 0.13 | 0.15 |
| Treatment[T.ORF3a] | 1.127 | 0.048 | 23.62 | 2.2e−123 | 1.033 | 1.220 | 3.09 | 2.81 | 3.39 |
| Time_scaled | 0.698 | 0.034 | 20.26 | 2.7e−91 | 0.631 | 0.766 | 2.01 | 1.88 | 2.15 |
| Time_scaled:treatment | −0.278 | 0.046 | −6.08 | 1.2e−09 | −0.368 | −0.188 | 0.76 | 0.69 | 0.83 |
| B | | | | | | | | | |
| Intercept | −1.516 | 0.097 | −15.65 | 3.3e−55 | −1.706 | −1.326 | 0.22 | 0.18 | 0.27 |
| Treatment[T.ORF3a] | 1.457 | 0.110 | 13.30 | 2.2e−40 | 1.242 | 1.672 | 4.29 | 3.46 | 5.32 |
| Time_scaled | −0.014 | 0.078 | −0.18 | 0.855 | −0.168 | 0.139 | 0.99 | 0.85 | 1.15 |
| Time_scaled:treatment | 0.292 | 0.094 | 3.10 | 0.002 | 0.108 | 0.476 | 1.34 | 1.11 | 1.61 |
| C | | | | | | | | | |
| Intercept | −2.30 | 0.088 | −26.00 | 4.53e−149 | −2.47 | −2.13 | 0.099 | 0.083 | 0.11 |
| Marker[T.mRFP] | 0.65 | 0.11 | 5.83 | 5.22e−09 | 0.43 | 0.87 | 1.92 | 1.54 | 2.40 |

Next, we examined ASC speck composition within ASC+ cells (Fig. 2). Here, ORF3a induced a pronounced shift toward multi-speck phenotypes (OR $\approx$ 4.3, 95% CI 3.5–5.3, $p < 0.001$). Importantly, the time $\times$ ORF3a interaction was positive (OR $\approx$ 1.3), showing that the fraction of cells with $\geq$ 2 specks increased progressively over time under ORF3a, whereas LPS maintained the canonical single-speck distribution (Table 1B).

Together, these models reveal a consistent picture: ORF3a rapidly drives a high baseline of ASC+ cells and promotes multi-speck formation, while LPS pro-

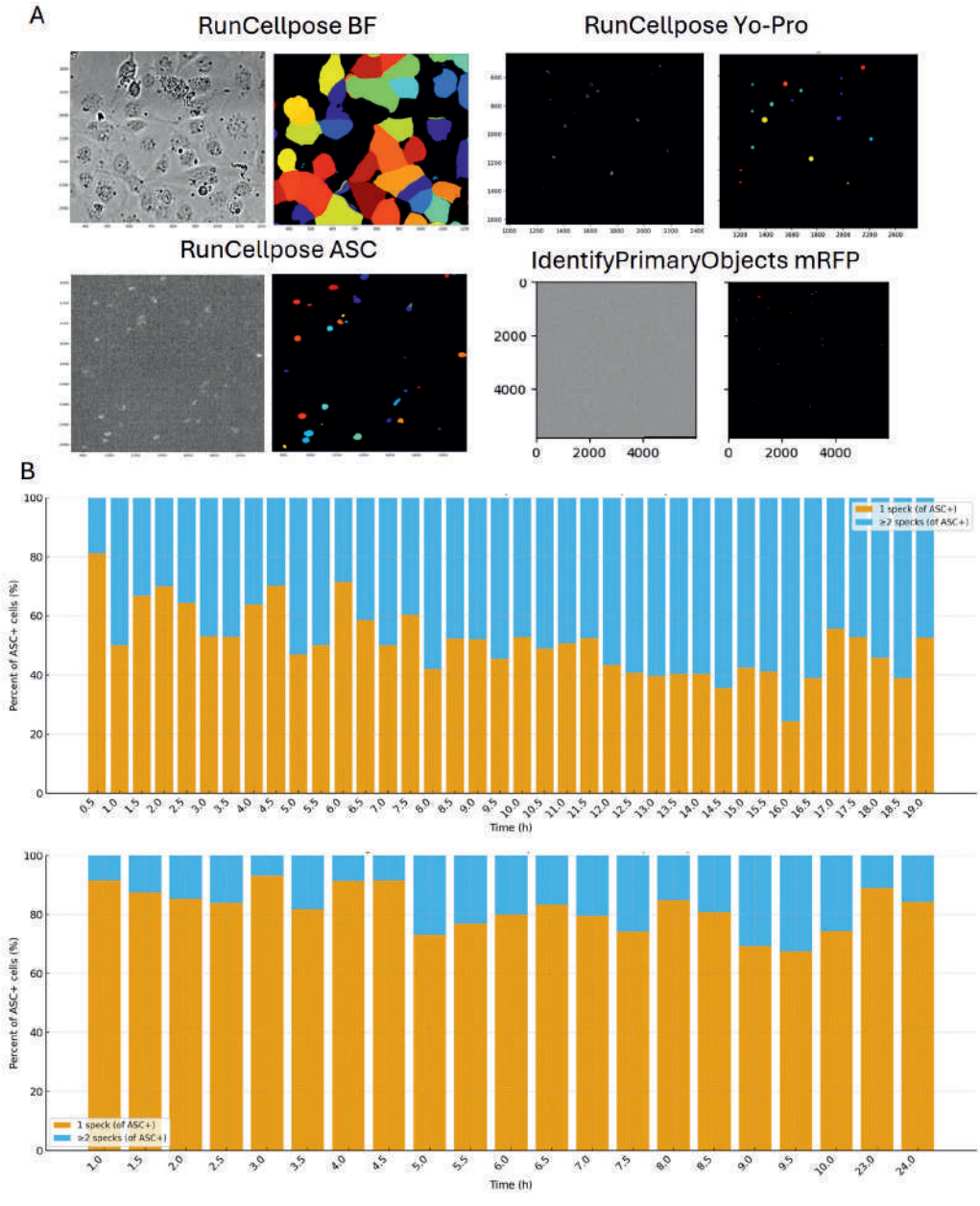


Fig. 2. 100% stacked composition of ASC specks within ASC-positive cells ORF3a (top) and LPS (bottom). Bars show the proportion of cells with 1 vs. $\geq 2$ ASC specks, normalized to the ASC-positive population at each time point (ASC+ $= \geq 1$ speck)

duces slower, time-dependent accumulation of ASC positivity dominated by single-speck phenotypes. Our data suggest ORF3a probably induces ASC-dependent direct caspase-1 activation, in pyroptosome type [1,7], while LPS-induced canoni-

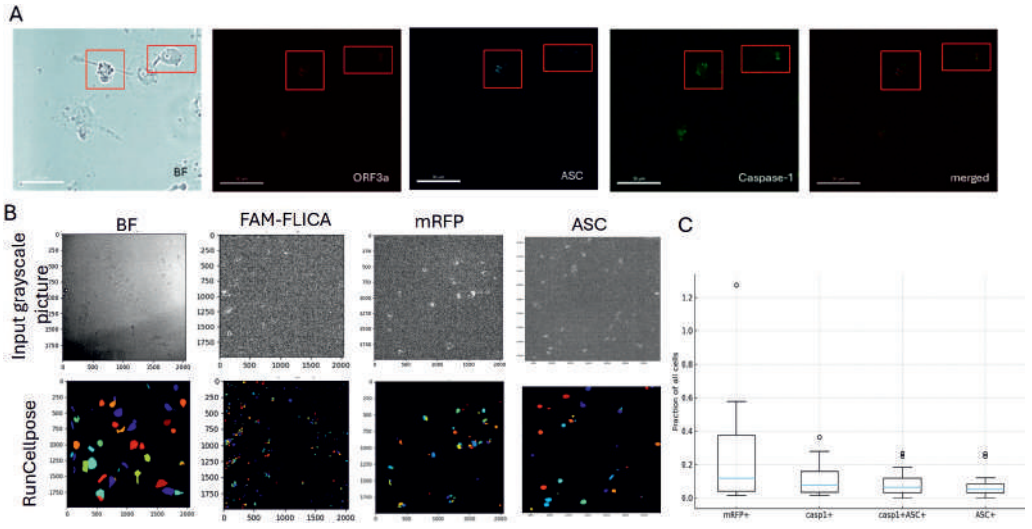


Fig. 3. (A) Representative images of transfected cells expressing ORF3a (mRFP, red). Individual channels are shown for ORF3a, ASC (blue), and caspase-1 (green), along with brightfield and merged images. Red boxes indicate cells in which ORF3a expression is accompanied by the formation of ASC specks and caspase-1 activation, suggesting inflammasome assembly. Scale bars, 50 µm. (B) Automated segmentation and quantification of ASC specks, caspase-1-positive cells, and total transfected cells via CellProfiler algorithm. For each channel (ASC, caspase-1, mRFP, BF), the original grayscale image is shown (top), alongside the corresponding segmented mask (bottom). (C) Marker-positive fractions across imaging fields. Boxplots show the distribution (median, interquartile range, and outliers) of fractions of cells positive for ORF3a-mRFP (transfected cells), caspase-1 (FAM-FLICA), caspase-1+ASC specks (triple-positive), and ASC specks (ORF3a+ASC+) calculated relative to the total number of cells per field. The data highlight that ORF3a-mRFP+ cells are the most abundant subset, whereas caspase-1 activation and ASC speck formation occur in progressively smaller fractions of the population

cal NLRP3-dependent caspase-1 pyroptotic activation. Our findings indicate that ORF3a expression promotes ASC speck assembly in a subset of cells, and that this process correlates with caspase-1 recruitment and activation (Fig. 3A). After image analysis (Fig. 3B) the graph shows that ORF3a-mRFP positivity was detected in $\sim$ 20–40% of cells per field, providing a baseline for transfection efficiency. Among these, ORF3a+caspase-1-positive cells represented a substantially smaller fraction ($\sim$ 5–15% of all cells) (Fig. 3C). The GLM confirmed a significant increase in the odds of caspase-1 activation in ORF3a-mRFP+ cells compared with baseline (OR $> 2.0$, $p < 0.001$), indicating that transfection strongly predisposes to inflammasome activation (Table 1C). Triple-positive ORF3a+casp1+ASC+ cells constituted a distinct subset ($\sim$ 5–10% of all cells), significantly less frequent than casp1+ cells alone but consistently above background, showing that ASC speck formation is enriched within casp1+ cells (GLM, OR $\approx$ 3–4, $p < 0.01$), supporting the conclusion that ASC assembly is functionally coupled to caspase-1 activation. By contrast, ORF3a+ASC+ cells lacking casp1 activation were rare ($< 5\%$), suggesting that ASC nucleation without caspase-1 is an uncommon route

in this system (Fig. 3C). Together, these distributions demonstrate a hierarchical reduction from ORF3a expression to caspase-1 activation and ASC assembly.

**Discussion.** Our data resolve distinct temporal and architectural features of ASC clustering in endothelial cells stimulated by canonical LPS/nigericin versus transfected with SARS-CoV-2 ORF3a. Consistent with the classical two-signal paradigm, LPS priming followed by a pore-forming second signal rapidly yields a single, perinuclear ASC speck per cell is the canonical inflammasome hub, producing synchronized ASC positivity and membrane permeabilization (YoPro-1) over time (reviewed in [8–10]). By contrast, ORF3a drives a slower, heterogeneous response with frequent multi-speck cells and an early high baseline of ASC+ that plateau, while the $\geq 2$ specks vs. one speck GLM shows a time-dependent enrichment of multi-speck phenotypes under ORF3a. These results indicate that ORF3a reconfigures the spatial program of ASC assembly away from a single hub toward multiple foci. Historically, the large ASC supramolecular assembly was termed the pyroptosome, a potent caspase-1 activating structure that forms one dominant punctum per cell [7]. However, more recent imaging and analysis show that active caspase-1 often resides in multiple small cytoplasmic complexes spatially segregated from the ASC speck, implying that the speck can act as a supramolecular organizing centre (SMOC) while caspase-1 activation propagates elsewhere [1]. Our ORF3a datasets align with this view: a sizeable fraction of caspase-1-positive cells lack visible ASC specks, whereas triple-positive (ORF3a+casp1+ASC+) cells form a distinct but smaller subset. Together with the multi-speck enrichment under ORF3a, these findings support coexisting modes: a speck-centric (pyroptosome-like) and a distributed (inflammasome-like) activation of caspase-1 within the same population. Mechanistically, our observations are consistent with ORF3a acting as a viroporin that primes and activates NLRP3 via $K^+$ efflux and NEK7, with both ASC-dependent and ASC-independent routes to caspase-1 activation [11]. Prior work on SARS-CoV ORF3a further shows TRAF3-dependent ubiquitination of ASC to trigger NLRP3 [12]. In canonical settings, ASC/NLRP3 material is transported to a centrosomal/MTOC locale via HDAC6-dependent aggresome-like machinery, reinforcing the single-speck architecture [9] and recent cryo-ET work has begun to resolve the ultrastructure of ASC/caspase-1 assemblies [10]. Our ORF3a findings suggest this transport/organization logic can be bypassed or diversified, yielding multiple activation foci and a non-synchronous temporal profile.

**Conclusion.** In endothelial cells, ORF3a engages caspase-1 through dual architectural modes, where along with canonical pyroptosome-like pathway, a new, distributed, multifocal inflammasome pathway is added. Our data argue that viral viroporins reshape inflammasome topology, balancing centralized ASC hubs with dispersed caspase-1 active sites shows a duality with implications for amplification of IL-1 family signalling and pyroptosis under viral challenge [1, 11], with impact on cell death and viral evolution and pathogenicity.

**Acknowledgments.** We gratefully acknowledge Stela Todorova, a student at the University of Vienna, for her assistance in conducting parts of the experimental work.

## REFERENCES

[1] Nagar A., T. Rahman, J. A. Harton (2021) The ASC speck and NLRP3 inflammasome function are spatially and temporally distinct, Front. Immunol., **12**, 752482.
[2] Yang Y., H. Wang, M. Kouadir et al. (2019) Recent advances in the mechanisms of NLRP3 inflammasome activation and its inhibitors, Cell Death Dis., **10**(2), 128.
[3] Chen Y., X. Ye, G. Escames et al. (2023) The NLRP3 inflammasome: contributions to inflammation-related diseases, Cell Mol. Biol. Lett., **28**(1), 51.
[4] Gao Y., G. Xu, L. Ma et al. (2021) Icariside I specifically facilitates ATP or nigericin-induced NLRP3 inflammasome activation and causes idiosyncratic hepatotoxicity, Cell Commun. Signal., **19**(1), 13.
[5] Nagar A., R. A. DeMarco, J. A. Harton (2019) Inflammasome and caspase-1 activity characterization and evaluation: An imaging flow cytometer-based detection and assessment of inflammasome specks and caspase-1 activation, J. Immunol., **202**(3), 1003–1015.
[6] Vora S. M., J. Lieberman, H. Wu (2021) Inflammasome activation at the crux of severe COVID-19, Nat. Rev. Immunol., **21**(11), 694–703.
[7] Fernandes-Alnemri T., J. Wu, J. W. Yu et al. (2007) The pyroptosome: a supramolecular assembly of ASC dimers mediating inflammatory cell death via caspase-1 activation, Cell Death Differ., **14**(9), 1590–1604.
[8] He Y., H. Hara, G. Nunez (2016) Mechanism and regulation of NLRP3 inflammasome activation, Trends Biochem. Sci., **41**(12), 1012–1021.
[9] Magupalli V. G., R. Negro, Y. Tian et al. (2020) HDAC6 mediates an aggresome-like mechanism for NLRP3 and pyrin inflammasome activation, Science, **369**(6510), eaas8995.
[10] Liu Y., H. Zhai, H. Alemayehu et al. (2023) Cryo-electron tomography of NLRP3-activated ASC complexes reveals organelle co-localization, Nat. Commun., **14**(1), 7246.
[11] Xu H., I. A. Akinyemi, S. A. Chitre et al. (2022) SARS-CoV-2 viroporin encoded by ORF3a triggers the NLRP3 inflammatory pathway, Virology, **568**, 13–22.
[12] Siu K. L., K. S. Yuen, C. Castano-Rodriguez et al. (2019) Severe acute respiratory syndrome coronavirus ORF3a protein activates the NLRP3 inflammasome by promoting TRAF3-dependent ubiquitination of ASC, FASEB J., **33**(8), 8865–8877.

[1]*Laboratory of Reproductive Omics Technologies, Institute of Biology and Immunology of Reproduction "Acad. Kiril Bratanov", Bulgarian Academy of Sciences, 73 Tsarigradsko Shosse Blvd, 1113 Sofia, Bulgaria*
*e-mails*: marienko@ibir.bas.bg
shayrabedyan@ibir.bas.bg (https://orcid.org/0000-0002-2147-1982)
ktodorova@ibir.bas.bg (https://orcid.org/0000-0002-4841-9156)

[2]*Department of Pharmacology, Pharmacy Faculty, Medical University-Pleven, 1 St. Kliment Ohridski St, 5800 Pleven, Bulgaria*
*e-mail*: pendicheva@gmail.com